

Thermodynamic potentials of metallic alloys in the undercooled liquid and solid glassy states

A.S. Makarov^a, R.A. Konchakov^a, N.P. Kobelev^b, V.A. Khonik^a

^a*Department of General Physics, State Pedagogical University, Lenin Street 86, Voronezh 394043, Russia*

^b*Institute of Solid State Physics, Russian Academy of Sciences, Chernogolovka, Moscow district 142432, Russia*

Abstract

We first present a comparative analysis of temperature evolution of the excess thermodynamic potentials (state functions), the enthalpy ΔH , entropy ΔS and Gibbs free energy $\Delta \Phi$, determined for *i*) undercooled melts using literature data and *ii*) solid glassy state calculated on the basis of calorimetry measurements using an approach proposed recently. Three metallic alloys were taken as an example for data analysis. It is found that temperature dependences $\Delta H(T)$, $\Delta S(T)$ and $\Delta G(T)$ calculated with both approaches coincide in the supercooled liquid range (i.e. at temperatures $T_g < T < T_x$, where T_g and T_x are the glass transition and crystallization onset temperatures, respectively). However, the necessary conditions for this coincidence is the introduction of important changes to the above approach *i*), which are related to the calculation of the melting entropy. We also introduce and calculate a dimensionless order parameter ξ , which changes in the range $0 < \xi < 1$ and characterizes the evolution of the structural order from liquid-like to crystal-like one. It is shown that the order parameter ξ_{scl} calculated for the end of the supercooled liquid range (i.e. for a temperature just below T_x) correlates with the melt critical cooling rate R_c : the smaller the order parameter ξ_{scl} (i.e. the closer the structure to that of the equilibrium liquid), the smaller R_c is.

Keywords: metallic glasses, calorimetry, thermodynamic potentials, order parameter, critical cooling rate

1. Introduction

The appearance of metallic glasses (MGs) produced by rapid melt solidification has sparked a new interest in the study of nucleation and crystal growth kinetics in undercooled melts [1–4]. An important parameter in the theory of nucleation is the difference between the Gibbs free energy of a melt and that

Email address: v.a.khonik@yandex.ru (V.A. Khonik)

of a solid crystalline phase. This difference is known as the excess Gibbs free energy of the liquid relative to the crystalline state [5–7]. The fundamental thermodynamic relations allow us to calculate the excess Gibbs free energy of a liquid, $\Delta\Phi_{L-X}(T)$, with respect to its crystalline state based on the known difference in specific heat capacities between the liquid and solid phases at constant pressure, $\Delta C_p^{L-X}(T) = C_p^L(T) - C_p^X(T)$ [8]. Meanwhile, the temperature dependence of the specific heat difference $\Delta C_p^{L-X}(T)$ over the entire range of the undercooled melt's existence is rarely available. At best, the specific heat difference $\Delta C_p^{L-X}(T)$ can be measured near the melting point T_f as well as near the glass transition temperature T_g .

Therefore, models have been developed to estimate the excess Gibbs free energy $\Delta\Phi_{L-X}(T)$, which include polynomial approximations of $\Delta C_p^{L-X}(T)$ and experimentally determinable parameters such as the melting point T_f , enthalpy of melting ΔH_f and entropy of melting ΔS_f . Currently, the most popular approach uses experimental data on the specific heat of the melt $C_p^L(T)$ and crystal $C_p^X(T)$ near T_f and T_g , which approximated by the polynomials [9]

$$C_p^L(T) = 3R + aT + bT^{-2}, \quad (1)$$

$$C_p^X(T) = 3R + cT + dT^2, \quad (2)$$

where R is the universal gas constant, a and b are the fitting parameters for the melt (L), c and d are the fitting parameters for the crystal (X). Polynomials (1) and (2) allow calculating temperature dependence of the difference $\Delta C_p^{L-X}(T)$ between the specific heat of the supercooled melt and that of the crystal over the entire range of the existence of the supercooled melt [10–14]. In turn, the quantity $\Delta C_p^{L-X}(T)$ allows determination of the excess enthalpy $\Delta H_{L-X}(T)$, excess entropy $\Delta S_{L-X}(T)$ and excess Gibbs free energy $\Delta\Phi_{L-X}(T)$ of the undercooled melt with respect to the crystal using the relations [15]:

$$\Delta H_{L-X}(T) = \Delta H_f - \int_T^{T_f} \Delta C_p^{L-X}(T) dT, \quad (3)$$

$$\Delta S_{L-X}(T) = \Delta S_f - \int_T^{T_f} \frac{\Delta C_p^{L-X}(T)}{T} dT, \quad (4)$$

$$\Delta\Phi_{L-X}(T) = \Delta H_{L-X}(T) - T\Delta S_{L-X}(T), \quad (5)$$

where all quantities are described above.

On the other hand, equations defining the excess thermodynamic potentials of MGs both in the *solid* (i.e. below T_g) and supercooled liquid (i.e. above T_g) states with respect to the crystalline counterpart are proposed in Refs [16–18]. The relations for excess enthalpy $\Delta H_{G-X}(T)$, excess entropy $\Delta S_{G-X}(T)$, and excess Gibbs free energy $\Delta\Phi_{G-X}(T)$ of glass with respect to the crystal have the form [16–18]:

$$\Delta H_{G-X}(T) = \frac{1}{\dot{T}} \int_T^{T_{cr}} \Delta W_{G-X}(T) dT, \quad (6)$$

$$\Delta S_{G-X}(T) = \frac{1}{\dot{T}} \int_T^{T_{cr}} \frac{\Delta W_{G-X}(T)}{T} dT, \quad (7)$$

$$\Delta \Phi_{G-X}(T) = \int_T^{T_{cr}} \Delta S_{G-X}(T) dT, \quad (8)$$

where \dot{T} is the heating rate, T_{cr} is the temperature of the complete crystallization, $\Delta W_{G-X}(T)$ constitutes the difference between the heat flow coming from glass $W_G(T)$ and its crystalline counterpart $W_X(T)$ and hereafter termed as the differential heat flow, i.e. $\Delta W_{G-X}(T) = W_G(T) - W_X(T)$. These equations allow calculating temperature dependences $\Delta H_{G-X}(T)$, $\Delta S_{G-X}(T)$ and $\Delta \Phi_{G-X}(T)$ from a low temperature (e.g. from room temperature) up to T_{cr} . It should be emphasized that if current temperature $T = T_{cr}$, then the integrals (6)–(8) become zero, and therefore, the quantities ΔH_{G-X} , ΔS_{G-X} and $\Delta \Phi_{G-X}(T)$ describe solely the excess enthalpy, entropy and Gibbs free energy of the glass compared to its crystalline counterpart.

While the analysis based on Eqs (3)–(5) has been used for a long time [15], relations (6)–(8) constitute a novel approach, which provides new interesting results [16–22]. It is, therefore, important to check whether these two approaches give consistent data in the common temperature range (i.e. at temperatures from T_g up to the crystallization onset temperature T_x). This is the first goal of the present investigation. Besides that, we perform a comparative analysis of these two methods in the explanation of MGs' glass-forming ability and revealed their advantages and shortcomings.

2. Experimental

The experimental part of the present investigation was performed on bulk glassy (at.%) $\text{Pd}_{40}\text{Ni}_{40}\text{P}_{20}$, $\text{Pt}_{42.5}\text{Cu}_{27}\text{Ni}_{9.5}\text{P}_{21}$ and high-entropy $\text{Zr}_{35}\text{Hf}_{13}\text{Al}_{11}\text{Ag}_8\text{Ni}_8\text{Cu}_{25}$ (the mixing entropy $\Delta S_{mix}/R=1.63$). The first alloy was prepared by direct melting of Pd (purity 99.95%) and Ni_2P (purity 99.5%) using alumina crucible in a pure Ar atmosphere and next treated in B_2O_3 flux. The second alloy was produced by direct remelting of the constituent elements (at least 99.9% pure) in evacuated quartz vial using a two-temperature method. High-entropy $\text{Zr}_{35}\text{Hf}_{13}\text{Al}_{11}\text{Ag}_8\text{Ni}_8\text{Cu}_{25}$ alloy was prepared by direct remelting of the elements (purity not worse than 99.9%) in an induction furnace in a pure Ar atmosphere. All glasses were prepared by melt jet quenching. The non-crystallinity of samples was verified by X-rays. For all compositions, the data on the specific heat of the melt (C_p^L) and crystal (C_p^X), melting point (T_f) and glass transition temperature (T_g) are available in the literature [23–26].

Excess thermodynamic potentials (Eqs (6)–(8)) were determined for the relaxed (preannealed) state of all MGs using differential scanning calorimetry

(DSC) data derived by a Hitachi DSC 7020 instrument operating in high-purity (99.999 %) N₂ atmosphere at a rate of 3 K/min. Every glass was tested according to the following protocol: *i*) an initial sample was heated up to the temperature of the complete crystallization T_{cr} with an empty reference DSC cell; this crystallized sample was next moved to the reference DSC cell; *ii*) a new sample in the initial state was heated into the supercooled liquid state (i.e. into the range $T_g \leq T < T_x$, where T_x is the crystallization onset temperature) (run 1) and cooled back to room temperature at about same rate of 3 K/min; *iii*) the same (relaxed) sample was tested up to T_{cr} (run 2) and, finally, *iv*) the same (crystallized) specimen is again heated up to T_{cr} (run 3). This protocol allows performing DSC measurements with the reference cell containing fully crystallized sample of approximately the same mass (50–70 mg) so that the measured heat flow during run 3 constitutes the difference between the heat flow coming from the relaxed glass $W_G(T)$ and its crystalline counterpart $W_X(T)$, i.e. the differential heat flow $\Delta W_{G-X}(T) = W_G(T) - W_X(T)$. The DSC instrument was calibrated using the melting points and enthalpies of 99.99 % pure In, Sn and Pb. The uncertainty in the enthalpy changes was estimated to be about 4%. The nitrogen flow rate was 60 ml/min. Under the above conditions, no visible oxidation of samples was detected.

3. Results and discussion

3.1. Thermodynamic potentials of undercooled melts

Figure 1 shows literature data on temperature dependences of the excess enthalpy $\Delta H_{L-X}(T)$, excess entropy $\Delta S_{L-X}(T)$ and excess Gibbs free energy $\Delta \Phi_{L-X}(T)$ for undercooled melts of Pd₄₀Ni₄₀P₂₀ [23, 24] (a,b), Pt_{42.5}Cu₂₇Ni_{9.5}P₂₁ [25] (c,d) and Zr₃₅Hf₁₃Al₁₁Ag₈Ni₈Cu₂₅ [26] (e,f) with respect to the crystalline state obtained with equations (3)–(5).

As an example, let us consider the data on Pt_{42.5}Cu₂₇Ni_{9.5}P₂₁ alloy shown in Fig.1 (c,d). The specific heat of the glassy, liquid and crystalline states of this alloy was studied in Ref.[25]. Temperature dependences of the heat capacities were approximated by polynomials (1) and (2) with $a = 11.5852 \times 10^{-3} \text{ Jmol}^{-1}\text{K}^{-2}$, $b = 5.1317 \times 10^6 \text{ Jmol}^{-1}\text{K}$, $c = -7.2702 \times 10^{-3} \text{ Jmol}^{-1}\text{K}^{-2}$ and $d = 16.5269 \times 10^{-6} \text{ Jmol}^{-1}\text{K}^{-3}$ [25]. After that, temperature dependence of the difference in the specific heats of the supercooled melt and crystal $\Delta C_p^{L-X}(T)$ was determined and further used to calculate the excess thermodynamic potentials of the supercooled melt using equations (3)–(5).

The melting temperature T_f and melting enthalpy ΔH_f were determined by DSC method at a heating rate of 20 K/min. The melting temperature was accepted as the liquidus temperature T_L . The melting enthalpy ΔH_f was determined from the heat flow $W(t, T)$ using the equation

$$\Delta H_f = \int_{T_S}^{T_L} \frac{W(t, T)}{\dot{T}} dT, \quad (9)$$

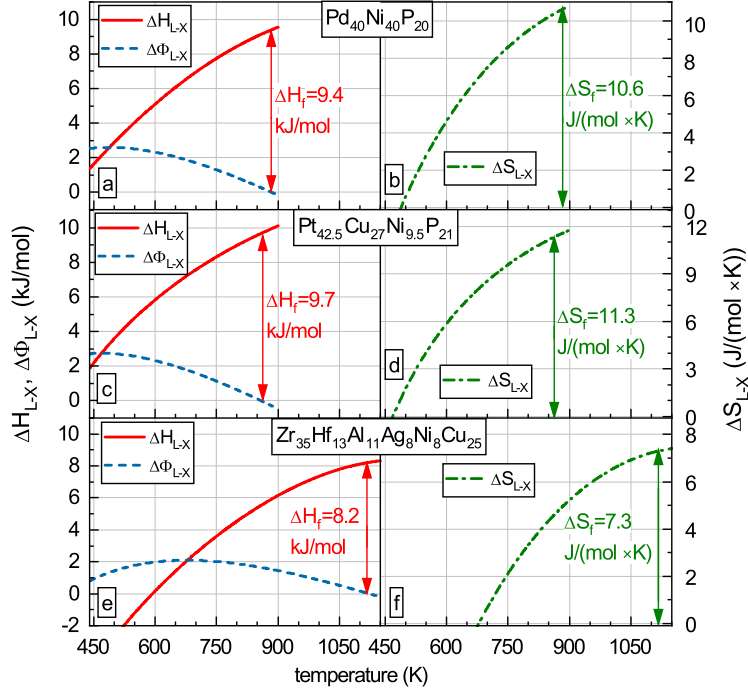


Figure 1: Temperature dependences of the excess enthalpy ΔH_{L-X} , excess entropy ΔS_{L-X} and excess Gibbs free energy $\Delta \Phi_{L-X}$ of $\text{Pd}_{40}\text{Ni}_{40}\text{P}_{20}$ (a,b) [23, 24]), $\text{Pt}_{42.5}\text{Cu}_{27}\text{Ni}_{9.5}\text{P}_{21}$ (c,d) [25] and $\text{Zr}_{35}\text{Hf}_{13}\text{Al}_{11}\text{Ag}_8\text{Ni}_8\text{Cu}_{25}$ (e,f) [26] undercooled melts with respect to the crystalline state obtained with equations (3)–(5). The enthalpy ΔH_f (Eq. 9) and entropy ΔS_f (Eq.(10)) at liquidus temperatures T_L are shown by the red and green arrows, respectively.

where $T_S=799$ K and $T_L=863$ K are the solidus and liquidus temperatures, respectively. The entropy of melting ΔS_f was defined as the ratio of the enthalpy of melting ΔH_f to the liquidus temperature,

$$\Delta S_f = \frac{\Delta H_f}{T_L}. \quad (10)$$

Next, using Eqs (9) and (10), the quantities $\Delta H_f=9.7$ kJmol $^{-1}$ and $\Delta S_f=11.3$ Jmol $^{-1}$ K $^{-1}$ were obtained. The enthalpy of melting ΔH_f and entropy of melting ΔS_f at the liquidus temperatures T_L are indicated in Fig.1(c,d) by the red and green arrows, respectively. It is seen that the excess enthalpy and entropy of $\text{Pt}_{42.5}\text{Cu}_{27}\text{Ni}_{9.5}\text{P}_{21}$ melt decrease as the undercooling increases. The excess Gibbs free energy $\Delta \Phi_{L-X}(T)$ is plotted in Fig.1(c).

Similar data on the thermodynamic potentials for other two alloys are given in panels (a,b) and (e,f) of Fig.1. The main conclusion from the data exemplified by Fig.1 is based on $\Delta \Phi_{L-X}$ -values taken at temperatures $(0.4-0.6) \times T_L$, where $\Delta \Phi_{L-X}$ reaches its maximum. It is believed that the small excess Gibbs free energy near these maxima reflect the small driving force for melt crystallization

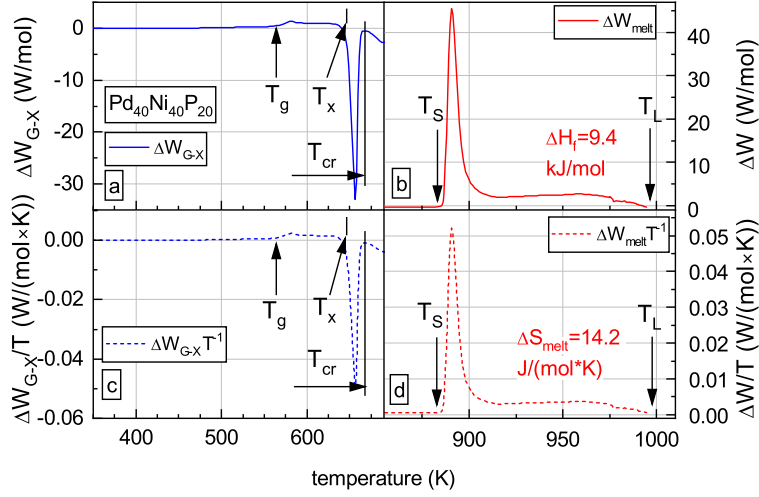


Figure 2: (a) Differential heat flow $\Delta W_{G-X}(T)$ of glassy $\text{Pd}_{40}\text{Ni}_{40}\text{P}_{20}$ up to the temperature of the complete crystallization T_{cr} . (b) DSC thermogram $\Delta W(T)$ of the same alloy after crystallization up to the liquidus temperature T_L . (c) The same data as in panel (a) but divided by the absolute temperature, i.e. $\Delta W_{G-X}(T)/T$. (d) The same data as in panel (b) but divided by the absolute temperature, i.e. $\Delta W(T)/T$. The characteristic temperatures T_g (glass transition), T_x (crystallization onset), T_{cr} , T_S (solidus) and T_L are indicated.

and, therefore, is crucial for understanding the high glass-forming ability of these melts [11, 12, 14, 25, 26]. We will return to this conclusion below and show that it is not supported by the experimental data analyzed in this work.

3.2. Enthalpies of glasses and undercooled melts

Let us now consider the enthalpy of the same alloys in the solid glassy state. Fig.2(a) shows temperature dependence of the differential heat flow $\Delta W_{G-X}(T)$ of relaxed $\text{Pd}_{40}\text{Ni}_{40}\text{P}_{20}$ glass derived in the present investigation. The relaxation was performed by heating of initial sample up to 610 K (which corresponds to the supercooled liquid state) and subsequent controlled cooling to room temperature.

The data in Fig.2(a) were used to calculate the excess enthalpy $\Delta H_{G-X}(T)$ with Eq.(6), which is shown in Fig.3(a). It is seen that $\Delta H_{G-X}(T)$ (light blue symbols) remains approximately constant up to T_g , rapidly increases in the supercooled liquid state (i.e. at $T_g \leq T \leq T_x$) and finally sharply falls down to zero due to full crystallization at $T_{cr} = 668$ K (indicated by the arrow in Fig. 2(a)). Red solid curve in Fig.3(a) gives the excess melt enthalpy $\Delta H_{L-X}(T)$ for the same alloy system replotted from Refs [23, 24]. It is seen that the glass excess enthalpy $\Delta H_{G-X}(T)$ and melt excess enthalpy $\Delta H_{L-X}(T)$ fully coincide in their common temperature range $T_g \leq T \leq T_x$. This means that these quantities agree with each other.

Panels (c) and (e) in Fig.3 show analogous data set for the alloys $\text{Pt}_{42.5}\text{Cu}_{27}\text{Ni}_{9.5}\text{P}_{21}$ and $\text{Zr}_{35}\text{Hf}_{13}\text{Al}_{11}\text{Ag}_8\text{Ni}_8\text{Cu}_{25}$, respectively. The excess entropy $\Delta H_{G-X}(T)$ for

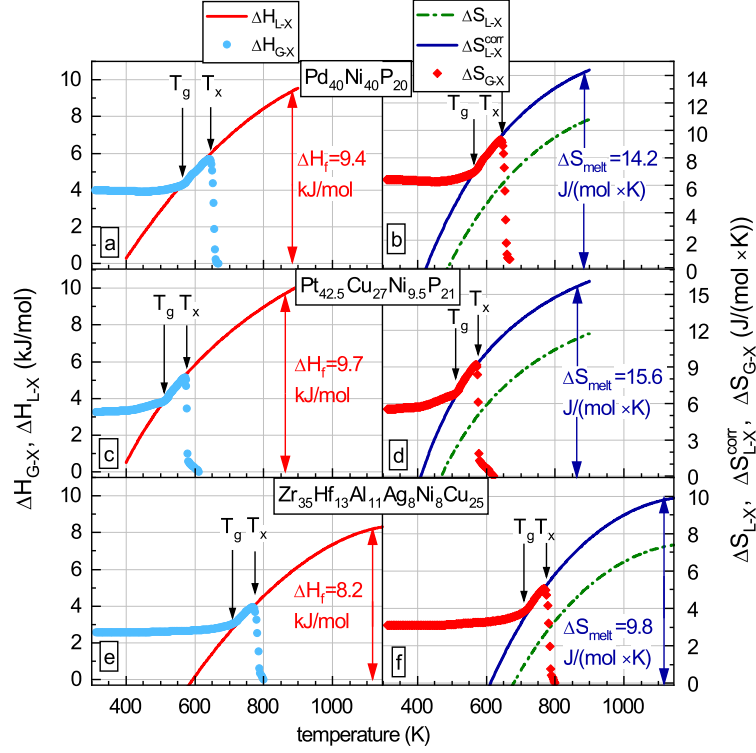


Figure 3: Temperature dependences of the excess enthalpies and excess entropies for the undercooled melts (labelled $L - X$) and glasses (labelled $G - X$): *i*) the excess enthalpy $\Delta H_{L-X}(T)$, excess entropy $\Delta S_{L-X}(T)$ and corrected excess entropy $\Delta S_{L-X}^{corr}(T)$ calculated using Eqs (3), (4) and (12), respectively; *ii*) the excess enthalpy $\Delta H_{G-X}(T)$ and excess entropy $\Delta S_{G-X}(T)$ determined with Eqs (6) and (7), respectively. Panels (a,b), (c,d) and (e,f) correspond to the alloys $\text{Pd}_{40}\text{Ni}_{40}\text{P}_{20}$, $\text{Pt}_{42.5}\text{Cu}_{27}\text{Ni}_{9.5}\text{P}_{21}$ and $\text{Zr}_{35}\text{Hf}_{13}\text{Al}_{11}\text{Ag}_8\text{Ni}_8\text{Cu}_{25}$, respectively. The glass transition temperatures T_g and crystallization onset temperatures T_x are shown. The melting enthalpy ΔH_f (Eq.9) and melting entropy ΔS_{melt} (Eq.(11)) are indicated.

the glassy state (light blue curves) was calculated using Eq.(6) on the basis of DSC data derived in the present investigation as described above. The excess entropy $\Delta H_{L-X}(T)$ (red curves) for $\text{Pt}_{42.5}\text{Cu}_{27}\text{Ni}_{9.5}\text{P}_{21}$ and $\text{Zr}_{35}\text{Hf}_{13}\text{Al}_{11}\text{Ag}_8\text{Ni}_8\text{Cu}_{25}$ undercooled melts was taken from Refs [25] and [26], respectively. It is seen that the enthalpies ΔH_{G-X} and ΔH_{L-X} coincide in their common range $T_g \leq T \leq T_x$, just in the above case of $\text{Pd}_{40}\text{Ni}_{40}\text{P}_{20}$ alloy.

3.3. Entropies of glasses and undercooled melts

To calculate the excess entropy of glass ΔS_{G-X} with Eq.(7), one needs the data on the differential heat flow divided by temperature, i.e. $\Delta W_{G-X}/T$, which is shown in Fig.2(c) for glassy $\text{Pd}_{40}\text{Ni}_{40}\text{P}_{20}$. The result of this calculation is given in Fig.3(b) by red symbols. In a qualitative sense, temperature change

of the entropy $\Delta S_{G-X}(T)$ follows the same pattern as the excess enthalpy described above (see Fig.3(a), light blue symbols). For a comparison, we also plotted the melt excess entropy $\Delta S_{L-X}(T)$ derived in Refs.[23, 24] for the same alloy system, see dash-dotted green curve in Fig.3(b). It is seen that the melt excess entropy $\Delta S_{L-X}(T)$ is far from being equal to the glass excess entropy $\Delta S_{G-X}(T)$ in the supercooled liquid region (i.e. in the range $T_g \leq T \leq T_x$).

The reason of this discrepancy seems to be quite clear. Upon calculation of the melt excess enthalpy $\Delta H_{L-X}(T)$ with Eq.(3), the authors [23, 24] use the the melting enthalpy ΔH_f , which was determined by integrating the heat flow data $W(t, T)$ according to Eq.(9), and got a melting enthalpy of 9.4 kJ/mol. This fully agrees with our experiment. Indeed, Fig.2(b) shows the heat flow of crystalline alloy $\text{Pd}_{40}\text{Ni}_{40}\text{P}_{20}$ in the temperature range $850 \text{ K} \leq T \leq 1000 \text{ K}$. Then, the application of Eq.(9) yields the same melting enthalpy $\Delta H_f = 9.4 \text{ kJ/mol}$. Accordingly, the excess enthalpies of melt $\Delta H_{L-X}(T)$ and glass $\Delta H_{G-X}(T)$ coincide in the supercooled liquid state, as mentioned above.

However, the situation with the melting entropies is different. To calculate the melting entropy ΔS_f , the authors [23, 24] used the ratio of the melting enthalpy to the solidus temperature given by Eq.(10) and arrive to a melting entropy $\Delta S_f = 10.6 \text{ Jmol}^{-1}\text{K}^{-1}$ as indicated in Fig.1(b). Next, using Eq.(4) they determined temperature dependence of the melt excess entropy $\Delta S_{L-X}(T)$, which is shown by green dash-dotted line in Fig.3(a). It is seen that in the temperature range of interest ($T_g \leq T \leq T_x$) this entropy lies far below the excess entropy of glass $\Delta S_{G-X}(T)$ calculated with Eq.(7) and shown by the red symbols in Fig.3(b). We believe that this inconsistency is due to the incorrect use of Eq.(10) to calculate the melting entropy: according to general thermodynamics [27], the differential of the entropy $dS = \delta Q/T$ (δQ is the elementary heat) and, therefore, the macroscopic entropy change must be calculated as an integral, $\Delta S = \int \delta Q/T$. Consequently, the melting entropy should be accepted as [20]

$$\Delta S_{melt} = \frac{1}{T} \int_{T_s}^{T_L} \frac{\Delta W(T)}{T} dT. \quad (11)$$

Figure 2(d) shows $\Delta W(T)/T$ -dependence for crystalline $\text{Pd}_{40}\text{Ni}_{40}\text{P}_{20}$ in the range from 850 K to 1000 K. Using this dependence together with Eq.(11), one can find the melting entropy $\Delta S_{melt} = 14.2 \text{ Jmol}^{-1}\text{K}^{-1}$.

Now let us rewrite formula (4) and define the corrected entropy difference between the undercooled liquid and crystalline phases as

$$\Delta S_{L-X}^{corr}(T) = \Delta S_{melt} - \int_T^{T_f} \frac{\Delta C_P^{L-X}(T)}{T} dT, \quad (12)$$

where ΔS_{melt} (determined by Eq.(11)) is used instead of ΔS_f in Eq.(4). Next, using this equation together with $\Delta C_P^{L-X}(T)$ -data from Refs [23, 24], one can calculate the corrected temperature dependence of melt excess entropy $\Delta S_{L-X}^{corr}(T)$. The $\Delta S_{L-X}^{corr}(T)$ -dependence thus determined is shown by the dark blue curve in Fig.3(b). It is seen that the corrected melt excess entropy

$\Delta S_{L-X}^{corr}(T)$ completely coincides with the glass excess entropy $\Delta S_{G-X}(T)$ (red symbols) in the common temperature range $T_g \leq T \leq T_x$.

The calculations of glass excess entropies $\Delta S_{G-X}(T)$ using Eq.(7) for MGs $\text{Pt}_{42.5}\text{Cu}_{27}\text{Ni}_{9.5}\text{P}_{21}$ and $\text{Zr}_{35}\text{Hf}_{13}\text{Al}_{11}\text{Ag}_8\text{Ni}_8\text{Cu}_{25}$ are shown in panels (d) and (f) in Fig.3, respectively. These $\Delta S_{G-X}(T)$ -dependencies in general are pretty much similar to the case of glassy $\text{Pd}_{40}\text{Ni}_{40}\text{P}_{20}$ (see Fig.3(b)).

Panels (d) and (f) in this Figure also show the data on melt excess entropies $\Delta S_{L-X}(T)$ for $\text{Pt}_{42.5}\text{Cu}_{27}\text{Ni}_{9.5}\text{P}_{21}$ and $\text{Zr}_{35}\text{Hf}_{13}\text{Al}_{11}\text{Ag}_8\text{Ni}_8\text{Cu}_{25}$ (dash-dotted green curves) derived in Refs. [25] and [26], respectively. Again, it is seen that excess entropies of melts $\Delta S_{L-X}(T)$ lie far below the excess entropies $\Delta S_{G-X}(T)$ for corresponding glasses in the supercooled liquid region. The reason for this discrepancy seems to be the same as above: the melting entropies were erroneously determined as the ratios of the melting enthalpies to liquidus temperatures [25, 26], i.e. as $\Delta S_f = \Delta H_f/T_L$ (indicated by green arrows in Fig.1(d,f)).

Regretfully, DSC thermograms for $\text{Pt}_{42.5}\text{Cu}_{27}\text{Ni}_{9.5}\text{P}_{21}$ and $\text{Zr}_{35}\text{Hf}_{13}\text{Al}_{11}\text{Ag}_8\text{Ni}_8\text{Cu}_{25}$ alloys covering the melting region are not available. In the view of this, we corrected the melting entropy data in the following way. One can notice that the melting entropies ΔS_f and ΔS_{melt} for $\text{Pd}_{40}\text{Ni}_{40}\text{P}_{20}$ alloy differ by 35 %. Assuming the same difference for $\text{Pt}_{42.5}\text{Cu}_{27}\text{Ni}_{9.5}\text{P}_{21}$ and $\text{Zr}_{35}\text{Hf}_{13}\text{Al}_{11}\text{Ag}_8\text{Ni}_8\text{Cu}_{25}$, one can accept the melting entropy for these alloys to be $S_{melt} = 15.6$ and $9.8 \text{ Jmol}^{-1}\text{K}^{-1}$, respectively (see dark blue arrows in Fig.3(d,f)). These ΔS_{melt} -values together with $\Delta C_P^{L-X}(T)$ -data from Refs [25, 26] were further used to recalculate the melt excess entropy using Eq.(12). Figure 3 (d,f) shows temperature $\Delta S_{L-X}(T)$ -dependences thus determined for the last two allows (see dark blue curves). It is seen that the excess entropies of melts and corresponding glasses coincide in the supercooled liquid state.

Overall, one can conclude that after appropriate corrections the melt and glass entropies derived using different approaches agree with each other in the common temperature range.

3.4. Gibbs free energy of undercooled melts and glasses

Let us now consider the excess Gibbs free energy $\Delta\Phi$ of undercooled melts and glasses. Figure 4 shows literature data on temperature dependences of the excess Gibbs free energy $\Delta\Phi_{L-X}(T)$ of $\text{Pd}_{40}\text{Ni}_{40}\text{P}_{20}$ [23, 24], $\text{Pt}_{42.5}\text{Cu}_{27}\text{Ni}_{9.5}\text{P}_{21}$ [25] and $\text{Zr}_{35}\text{Hf}_{13}\text{Al}_{11}\text{Ag}_8\text{Ni}_8\text{Cu}_{25}$ [26] melts (dark blue dashed curves). This Figure also gives the Gibbs free energy $\Delta\Phi_{G-X}(T)$ of same glasses calculated using Eq.(8) (light blue curves). It is seen that the excess Gibbs free energy of undercooled melts $\Delta\Phi_{L-X}$ decreases with temperature at $T > T_g$ and becomes zero at the melting point. Meanwhile, the excess Gibbs free energy of glasses $\Delta\Phi_{G-X}$ also decreases with temperature without any features but goes to zero at $T = T_{cr}$. Thus, the excess Gibbs free energy $\Delta\Phi_{L-X}$ of undercooled melts is far different from the excess Gibbs free energy $\Delta\Phi_{G-X}$ of glasses.

However, recalling incorrect determination of the melting entropy ΔS_{L-X} described above, one should replace it by the corrected entropy ΔS_{L-X}^{corr} in

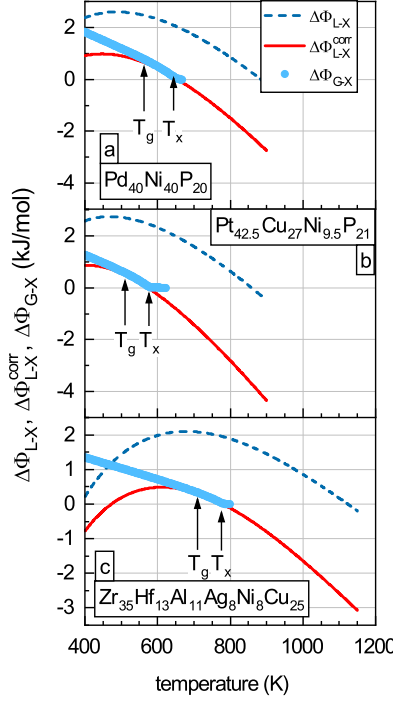


Figure 4: Temperature dependences of the excess Gibbs free energy $\Delta\Phi$ of undercooled melts (labelled $L - X$) and metallic glasses (labelled $G - X$) calculated by Eqs (5), (13) and (8) for the quantities $\Delta\Phi_{L-X}$, $\Delta\Phi_{L-X}^{corr}$ and $\Delta\Phi_{G-X}$, respectively. The data on $\Delta\Phi_{L-X}$ for $\text{Pd}_{40}\text{Ni}_{40}\text{P}_{20}$ (a), $\text{Pt}_{42.5}\text{Cu}_{27}\text{Ni}_{9.5}\text{P}_{21}$ (b) and $\text{Zr}_{35}\text{Hf}_{13}\text{Al}_{11}\text{Ag}_8\text{Ni}_8\text{Cu}_{25}$ (c) alloys are taken from Refs [23, 24], [25] and [26], respectively. The glass transition temperatures T_g and crystallization onset temperatures T_x are indicated.

Eq.(5), as argued in the previous Section. Then, instead of Eq.(5) one should write down an expression for the corrected excess Gibbs free energy of undercooled melt as

$$\Delta\Phi_{L-X}^{corr}(T) = \Delta H_{L-X}(T) - T\Delta S_{L-X}^{corr}(T), \quad (13)$$

where all the quantities are described above.

Then, taking $\Delta H_{L-X}(T)$ from Refs [23–26] together with corrected $\Delta S_{L-X}^{corr}(T)$ and using Eq.(13), one can determine corrected temperature dependence of the excess Gibbs free energy $\Delta\Phi_{L-X}^{corr}(T)$ of undercooled melts. The corresponding results are given by the red curves in Fig.4. It is seen that corrected $\Delta\Phi_{L-X}^{corr}(T)$ for the alloys under consideration coincides with the excess Gibbs free energy of corresponding glasses $\Delta\Phi_{G-X}(T)$ in the supercooled liquid region, i.e. at temperatures $T_g \leq T \leq T_x$.¹ Above the temperature of complete crystallization

¹It is to be noted that, generally speaking, Eqs (5) and (13) cannot be applied for a

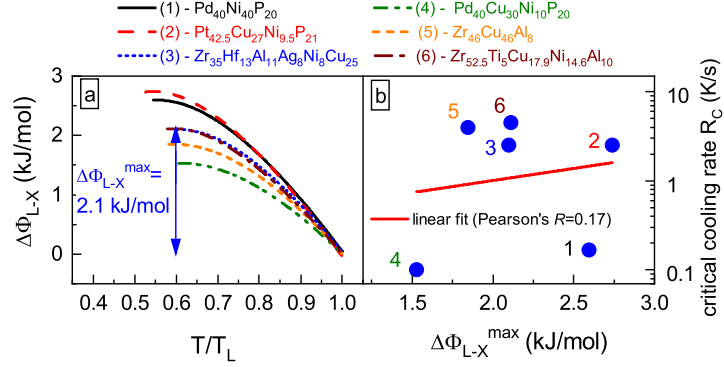


Figure 5: (a) – Temperature dependences of the excess Gibbs free energy $\Delta\Phi(T)_{L-X}$ of indicated undercooled melts as a function of the normalized temperature T/T_L . The maximal value on this dependence, $\Delta\Phi_{L-X}^{\max}$, for $\text{Zr}_{35}\text{Hf}_{13}\text{Al}_{11}\text{Ag}_8\text{Ni}_8\text{Cu}_{25}$ is indicated. (b) – The critical cooling rate R_c of the same melts as a function of $\Delta\Phi(T)_{L-X}^{\max}$. No clear correlation is seen.

T_{cr} , the Gibbs free energy $\Delta\Phi_{L-X}^{corr}$ becomes negative. This indicates negative work on the transformation of an undercooled melt into the crystal in the range $T_{cr} \leq T \leq T_L$.

3.5. On the correlation of undercooled melt Gibbs free energy and melt critical cooling rate

As mentioned above, it is suggested in the literature that small excess Gibbs free energy $\Delta\Phi_{L-X}$ at temperatures $(0.4 - 0.6) \times T_L$, corresponding to a maximum of this dependence, reflect a small driving force for melt crystallization and, therefore, should be indicative of good glass-forming ability (GFA) (e.g. Refs [11, 12, 14, 25, 26]). One can verify this suggestion for the alloys under consideration.

Figure 5(a) shows $\Delta\Phi_{L-X}$ as a function of the normalized temperature T/T_L . It is seen that, for instance, the maximum $\Delta\Phi_{L-X}^{\max}$ -value for undercooled $\text{Zr}_{35}\text{Hf}_{13}\text{Al}_{11}\text{Ag}_8\text{Ni}_8\text{Cu}_{25}$ melt is 2.1 kJmol⁻¹. Panel (b) in this Figure gives the critical cooling rate R_c , which is a direct measure of the GFA, plotted as a func-

description of an undercooled melt. Indeed, it is easy to show that thermodynamic relationship

$$\Delta\Phi = \Delta H - T\Delta S \quad (14)$$

is valid only for isothermal conditions. Meanwhile, Eqs (5) and (13) assume a varying temperature. For the latter case, by the definition of the Gibbs free energy [27], one should write down that $d\Delta\Phi = -\Delta SdT$ and, therefore,

$$\Delta\Phi = - \int \Delta SdT, \quad (15)$$

which is similar to the relationship (8) used to calculate glass excess Gibbs free energy [18]. However, numerical calculations with Eqs (14) and (15) give quite close results.

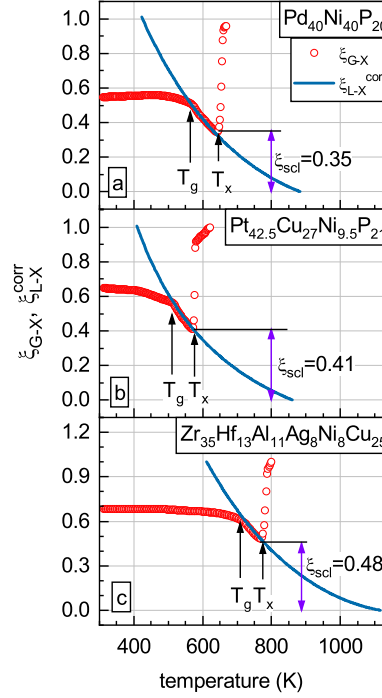


Figure 6: Temperature dependences of the order parameter for indicated undercooled melts (ξ_{L-X}^{corr}) and glasses (ξ_{G-X}). The values of ξ_{scl} , glass transition T_g and crystallization onset T_x temperatures are indicated.

tion of $\Delta\Phi_{L-X}^{max}$. The R_c -data for $\text{Zr}_{35}\text{Hf}_{13}\text{Al}_{11}\text{Ag}_8\text{Ni}_8\text{Cu}_{25}$, $\text{Pt}_{42.5}\text{Cu}_{27}\text{Ni}_{9.5}\text{P}_{21}$ and $\text{Pd}_{40}\text{Ni}_{40}\text{P}_{20}$ alloys are taken from Refs [26, 29, 30], respectively. The data on $\Delta\Phi_{L-X}^{max}$ and R_c for $\text{Pd}_{40}\text{Cu}_{30}\text{Ni}_{10}\text{P}_{20}$ [24, 30], $\text{Zr}_{46}\text{Cu}_{46}\text{Al}_8$ [14, 31] and $\text{Zr}_{52.5}\text{Cu}_{17.9}\text{Ni}_{14.6}\text{Al}_{10}\text{Ti}_5$ [31, 32] are taken from indicated references.

It is seen that *i*) any clear correlation between $\Delta\Phi_{L-X}^{max}$ and R_c is absent and *ii*) the alloys $\text{Pt}_{42.5}\text{Cu}_{27}\text{Ni}_{9.5}\text{P}_{21}$ and $\text{Zr}_{35}\text{Hf}_{13}\text{Al}_{11}\text{Ag}_8\text{Ni}_8\text{Cu}_{25}$, which have very close R_c 's, demonstrate nonetheless quite different $\Delta\Phi_{L-X}^{max}$ -values. These observations do not support the aforementioned idea that $\Delta\Phi_{L-X}^{max}$ is related to the GFA. To our knowledge, there is currently no other data available in the literature on a possible correlation between $\Delta\Phi_{L-X}^{max}$ and R_c .

3.6. Dimensionless entropy-based parameter of structural ordering and critical cooling rate

On the other hand, it was recently found that MGs' excess entropy correlates with the glass-forming ability of corresponding melts [18, 20]. In the view of this, it is reasonable to check if there is any correlation between the melt/glass excess entropy and the critical cooling rate R_c for the alloys under consideration.

Following the ideas presented in Ref.[20], one can introduce dimensionless parameters of structural order ξ_{L-X}^{corr} for an undercooled melt and corresponding

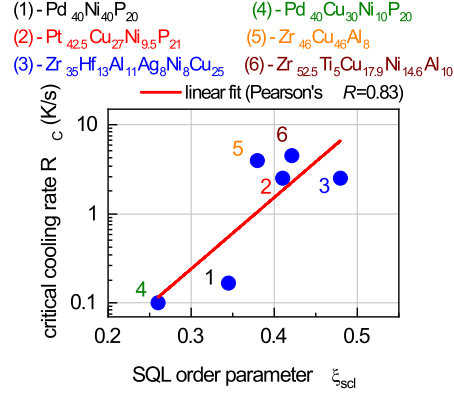


Figure 7: Critical cooling rate R_c for indicated melts as a function of the order parameter ξ_{scl} calculated with Eq.(17) for the end of the supercooled liquid region (see Fig.6).

glass ξ_{G-X} as

$$\xi_{L-X}^{corr}(T) = 1 - \frac{\Delta S_{L-X}^{corr}(T)}{\Delta S_{melt}}, \quad (16)$$

$$\xi_{G-X}(T) = 1 - \frac{\Delta S_{G-X}(T)}{\Delta S_{melt}}, \quad (17)$$

where ΔS_{L-X}^{corr} and ΔS_{G-X} are determined by Eqs (12) and (7), respectively, ΔS_{melt} is the entropy increase upon heating from the solidus T_S to liquidus T_L temperature as defined by Eq.(11). The order parameter varies in the range $0 < \xi_{L-X}^{corr}, \xi_{G-X} < 1$ upon changing the structure from the fully disordered (liquid-like) state with $\Delta S_{L-X}^{corr} \rightarrow \Delta S_{melt}$ or $\Delta S_{G-X} \rightarrow \Delta S_{melt}$ and $\xi_{L-X}^{corr}, \xi_{G-X} \rightarrow 0$ towards the fully ordered state (crystal-like) characterized by $\Delta S_{L-X}^{corr} \rightarrow 0$ or $\Delta S_{G-X} \rightarrow 0$ and $\xi_{L-X}^{corr}, \xi_{G-X} \rightarrow 1$.

It is interesting to calculate the order parameter for a temperature corresponding to the end of the supercooled liquid range, just before the crystallization onset at T_c . We denote this order parameter as ξ_{scl} hereafter. It was earlier shown that ξ_{scl} correlates with the melt critical cooling rate R_c . An increase of the structural order given by ξ_{scl} worsens the glass forming ability (i.e. increases R_c) [20]. It is important to check whether a similar situation holds for the alloys studied in the present work.

Figure 6 shows temperature dependences of structural order parameter for indicated undercooled melts $\xi_{L-X}^{corr}(T)$ (dark blue curves) and glasses $\xi_{G-X}(T)$ (red circles) calculated according to Eqs (16) and (17), respectively. For all alloys, the situation remains nearly the same: the order parameter ξ_{scl} remain approximately constant at low temperatures, next decreases upon further heating and reaches indicated minima in the end of supercooled liquid range due to structural disordering [20, 22]. Continued heating of glasses leads to an increase in $\xi_{G-X}(T)$ to unity at $T = T_{cr}$ because of crystallization. For undercooled

melts, the order parameter $\xi_{L-X}^{corr}(T)$ coincides with $\xi_{G-X}(T)$ in the supercooled liquid state (i.e. at $T_g \leq T \leq T_x$). At higher temperatures $T > T_x$, the order parameter of ξ_{L-X}^{corr} decreases with temperature and reaches zero at the melting point, as expected.

Figure 7 gives the critical cooling rate R_c as a function of the order parameter ξ_{scl} for the alloys under study. A clear increase of R_c with ξ_{scl} is seen. The best glass-forming material, $\text{Pd}_{40}\text{Cu}_{30}\text{Ni}_{10}\text{P}_{20}$, exhibits the smallest ξ_{scl} . Similar $\xi_{scl}(R_c)$ -dependence was previously found for a number of MGs [20]. Thus, structural disordering in the supercooled liquid state of glass reflects the ease of melt glass formation. The smaller the order parameter ξ_{scl} (i.e. the closer the structure to that of the equilibrium liquid), the lower the R_c is.

4. Conclusions

The study reports the first comparative analysis of temperature evolution of the excess thermodynamic potentials (enthalpy ΔH , entropy ΔS and Gibbs free energy $\Delta \Phi$) of three alloys taken as an example, $\text{Pd}_{40}\text{Ni}_{40}\text{P}_{20}$, $\text{Pt}_{42.5}\text{Cu}_{27}\text{Ni}_{9.5}\text{P}_{21}$ and $\text{Zr}_{35}\text{Hf}_{13}\text{Al}_{11}\text{Ag}_8\text{Ni}_8\text{Cu}_{25}$, in the undercooled molten state and solid glassy state. Excess thermodynamic potentials of undercooled melts with respect to the crystalline state, ΔH_{L-X} , ΔS_{L-X} and $\Delta \Phi_{L-X}$, are taken from the literature. For the glassy state, the excess enthalpy ΔH_{G-X} , entropy ΔS_{G-X} and Gibbs free energy $\Delta \Phi_{L-X}$ were calculated on the basis of calorimetry data using the method proposed recently.

It is found that temperature dependences of the excess enthalpies for undercooled melts and glasses, $\Delta H_{L-X}(T)$ and $\Delta H_{G-X}(T)$, coincide in the supercooled liquid range, i.e. at temperatures $T_g \leq T \leq T_x$ (where T_g and T_x are the glass transition and crystallization onset temperatures, respectively). Temperature dependences of the excess entropies, $\Delta S_{L-X}(T)$ and $\Delta S_{G-X}(T)$ also coincide in this temperature range but only after important corrections related to the calculations of the melting entropy. The Gibbs free energies of undercooled melts $\Delta \Phi_{L-X}(T)$ are also equal to glass Gibbs free energies $\Delta \Phi_{G-X}(T)$ in the supercooled liquid range provided that the same entropy corrections are applied.

We also studied the effect of the excess Gibbs free energy and entropy on the glass-forming ability (GFA), which is directly characterized by the melt critical cooling rate R_c . First, we found no clear relationship between R_c and melt excess Gibbs free energy at the maximum of the $\Delta \Phi_{L-X}(T)$ -dependence, contrary to what is suggested in the literature.

On the other hand, on the basis entropy data, we introduced a dimensionless order parameter ξ , which changes in the range $0 < \xi < 1$. It is shown that temperature dependences of this parameter determined with undercooled melt and glass entropy data coincide in the supercooled liquid range. It is also found that the order parameter ξ_{scl} calculated for the end of this temperature range (i.e. for a temperature just below T_x) correlates with the critical cooling rate: a decrease of structural order given by ξ_{scl} results in a decrease of R_c (i.e. leads to better GFA), in line with literature data.

Declaration of competing interests

The authors declare that they have no known competing financial interests or personal relationships that could have appeared to influence the work reported in this paper.

Acknowledgements

The work was supported by the Russian Science Foundation under the project No. 23-12-00162.

References

- [1] S. Karthika, T.K. Radhakrishnan, P. Kalaichelvi, A Review of Classical and Nonclassical Nucleation Theories, *Cryst. Growth Des.* 16 (2016) 6663-6681, <https://doi.org/10.1021/acs.cgd.6b00794>
- [2] J. H. Na, S. L. Corona, A. Hoff, W. L. Johnson, Observation of an apparent first-order glass transition in ultrafragile Pt-Cu-P bulk metallic glasses, *PNAS* 117 (2020) 2779, <https://doi.org/10.1073/pnas.1916371117>.
- [3] Y. Prabhu, A. K. Srivastav, D. V. Gunderov, J. Bhatt, Thermodynamic model to predict bulk metallic glass forming composition in Zr-Cu-Fe-Al system and understanding the role of Dy addition, *Physica B* 624 (2022) 413416, <https://doi.org/10.1016/j.physb.2021.413416>.
- [4] A. Kuball, O. Gross, B. Bochtler, I. Gallino, R. Busch, Thermodynamics, kinetics and crystallization behavior of the Pd₃₁Ni₄₂S₂₇ bulk glass forming alloy, *Intermetallics* 173 (2024) 1084222, <https://doi.org/10.1016/j.intermet.2024.108422>.
- [5] F.C. Frank, Supercooling of liquids, *Proc. Roy. Soc. Lond. A* 215 (1952) 43, <https://doi.org/10.1098/rspa.1952.0194>
- [6] D. Turnbull, J.C. Fisher, Rate of Nucleation in Condensed Systems, *J. Chem. Phys.* 17 (1949) 71-73, <https://doi.org/10.1063/1.1747055>
- [7] D. Turnbull, Formation of Crystal Nuclei in Liquid Metals, *J. Appl. Phys.* 21 (1950) 1022-1028, <https://doi.org/10.1063/1.1699435>
- [8] Y. Austin Chang, W. Alan Oates, *Materials Thermodynamics*, John Wiley & Sons, Inc., New Jersey, 2009, <https://doi.org/10.1002/9780470549940>
- [9] J.D. Hoffman, Thermodynamic driving force in nucleation and growth processes, *J. Chem. Phys.* 29 (1958) 1022-1028, <https://doi.org/10.1063/1.1744688>

- [10] R. Busch, Y.J. Kim, W.L. Johnson, Thermodynamics and kinetics of the undercooled liquid and the glass transition of the $\text{Zr}_{41.2}\text{Ti}_{13.8}\text{Cu}_{12.5}\text{Ni}_{10.0}\text{Be}_{22.5}$ alloy, *J. Appl. Phys.* 77 (1995) 4039, <https://doi.org/10.1063/1.359485>
- [11] R. Busch, W. Liu, W.L. Johnson, Thermodynamics and kinetics of the $\text{Mg}_{65}\text{Cu}_{25}\text{Y}_{10}$ bulk metallic glass forming liquid, *J. Appl. Phys.* 83 (1998) 4134, <https://doi.org/10.1063/1.367167>
- [12] R. Busch, The thermophysical properties of bulk metallic glass-forming liquids, *JOM* 52 (2000) 39–42, <https://doi.org/10.1007/s11837-000-0160-7>
- [13] B.A. Legg, J. Schroers, R. Busch, Thermodynamics, kinetics, and crystallization of $\text{Pt}_{57.3}\text{Cu}_{14.6}\text{Ni}_{5.3}\text{P}_{22.8}$ bulk metallic glass, *Acta Mater.* 55 (2007) 1109–1116, <https://doi.org/10.1016/j.actamat.2006.09.024>
- [14] Q.K. Jiang, X.D. Wang, X.P. Nie, G.Q. Zhang, H. Ma, H.-J. Fecht, J. Bendnarcik, H. Franz, Y.G. Liu, Q.P. Cao, J.Z. Jiang, Zr-(Cu,Ag)-Al bulk metallic glasses, *Acta Mater.* 56 (2008) 1785–1796, <https://doi.org/10.1016/j.actamat.2007.12.030>
- [15] C.V. Thompson, F. Spaepen, On the approximation of the free energy change on crystallization, *Acta Metall.* 27 (1979) 1855–1859, [https://doi.org/10.1016/0001-6160\(79\)90076-2](https://doi.org/10.1016/0001-6160(79)90076-2)
- [16] A.S. Makarov, G.V. Afonin, J.C. Qiao, A.M. Glezer, N.P. Kobelev, V.A. Khonik, Determination of the thermodynamic potentials of metallic glasses and their relation to the defect structure, *J. Phys.: Condens. Matter* 33 (2021) 435701, <https://doi.org/10.1088/1361-648X/ac18f1>
- [17] A.S. Makarov, M.A. Kretova, G.V. Afonin, J.C. Qiao, A.M. Glezer, N.P. Kobelev, V.A. Khonik, On the nature of the excess internal energy and entropy of metallic glasses, *JETP Lett.* 115 (2022) 102–107, <https://doi.org/10.1134/S0021364022020072>
- [18] A.S. Makarov, R.A. Konchakov, G.V. Afonin, J.C. Qiao, N.P. Kobelev, V.A. Khonik, Excess entropy of metallic glasses and its relation to the glass-forming ability of maternal melts, *JETP Lett.* 120 (2024) 759–765, <https://doi.org/10.1134/S0021364024602975>
- [19] R.A. Konchakov, A.S. Makarov, G.V. Afonin, J.C. Qiao, N.P. Kobelev, V.A. Khonik, Relation of the fragility of metallic glasses with the mixing entropy and excess entropy with respect to the maternal crystal, *JETP Lett.* 119 (2024) 458–463, <https://doi.org/10.1134/S0021364024600393alloy>.

- [20] A.S. Makarov, G.V. Afonin, R.A. Konchakov, V.A. Khonik, J.C. Qiao, A.N. Vasiliev, N.P. Kobelev, Dimensionless parameter of structural ordering and excess entropy of metallic and tellurite glasses, *Scr. Mater.* 239 (2024) 115783, <https://doi.org/10.1016/j.scriptamat.2023.115783>.
- [21] A.S. Makarov, J.B. Cui, J.C. Qiao, G.V. Afonin, N.P. Kobelev, V.A. Khonik, Relationship between the entropy of mixing, excess entropy and the shear viscosity of metallic glasses near the glass transition, *Intermetallics* 175 (2024) 108478 (<https://doi.org/10.1016/j.intermet.2024.108478>).
- [22] G.V. Afonin, A.S. Makarov, R.A. Konchakov, J.C. Qiao, A.N. Vasiliev, N.P. Kobelev, V. Khonik, Thermodynamic entropy-based parameter of structural disordering and its relation to the width of the X-ray structure factor and defect concentration in a metallic glass, *J. Alloys Compd.* 983 (2024) 173836 (<https://doi.org/10.1016/j.jallcom.2024.173836>).
- [23] G. Wilde, G.P. Görler, R. Willnecker, G. Dietz, Thermodynamic properties of $\text{Pd}_{40}\text{Ni}_{40}\text{P}_{20}$ in the glassy, liquid, and crystalline states, *Appl. Phys. Lett.* 65 (1994) 397–399, <https://doi.org/10.1063/1.112313>
- [24] I.-R. Lu, G. Wilde, Görler, R. Willnecker, Thermodynamic properties of Pd-based glass-forming alloys, *J. Non-Cryst.Sol.* 250-252 (1999) 577-581, [https://doi.org/10.1016/S0022-3093\(99\)00135-0](https://doi.org/10.1016/S0022-3093(99)00135-0)
- [25] N. Neuber, O. Gross, M. Frey, B. Bochtler, A. Kuball, S. Hechler, I. Gallino, R. Busch, On the thermodynamics and its connection to structure in the Pt-Pd-Cu-Ni-P bulk metallic glass forming system, *Acta Mater.* 220 (2021) 117300, <https://doi.org/10.1016/j.actamat.2021.117300>
- [26] Y. Ohashi, T. Wada, H. Kato, High-entropy design and its influence on glass-forming ability in Zr–Cu-based metallic glass, *J. Alloys Compd.* 915 (2022) 165366, <https://doi.org/10.1016/j.jallcom.2022.165366>
- [27] L. D. Landau, E. M. Lifshitz. *Statistical Physics. Vol. 5* (3rd ed.). Butterworth-Heineman, 1980.
- [28] A. Inoue, N. Nishiyama, H. Kimura, Preparation and thermal stability of bulk amorphous $\text{Pd}_{40}\text{Cu}_{30}\text{Ni}_{10}\text{P}_{20}$ alloy cylinder of 72 mm in diameter, *Mater. Trans. JIM* 38 (1997) 179-183, <https://doi.org/10.2320/matertrans1989.38.179>
- [29] O. Gross, S.S. Riegler, M. Stolpe, B. Bochtler, A. Kuball, S. Hechler, R. Busch, I. Gallino, On the high glass-forming ability of Pt-Cu-Ni/Co-P-based liquids, *Acta Mater.* 141 (2017) 109-119, <https://doi.org/10.1016/j.actamat.2017.09.013>

- [30] A. Inoue, N. Nishiyama, H. Kimura, Preparation and thermal stability of bulk amorphous $\text{Pd}_{40}\text{Cu}_{30}\text{Ni}_{10}\text{P}_{20}$ alloy cylinder of 72 mm in diameter, Mater. Trans. JIM 38 (1997) 179-183, <https://doi.org/10.2320/matertrans1989.38.179>
- [31] D. Xing, J. Sun, G. Wang, M. Yan, The relations between ΔT_x and the glass forming ability of bulk amorphous Zr-Cu-Ni-Al-Hf-Ti and $\text{Zr}_{52.5}\text{Cu}_{17.9}\text{Ni}_{14.6}\text{Al}_{10}\text{Ti}_5$ alloys, J. Alloys Compd. 375 (2004) 239-242, <https://doi.org/10.1016/j.jallcom.2003.11.155>
- [32] M. Motyka, E. Gilardi, G. Heunen, M. Baricco, Kinetics and thermodynamics of bulk glass formation in a $\text{Zr}_{52.5}\text{Cu}_{17.9}\text{Ni}_{14.6}\text{Al}_{10}\text{Ti}_5$ alloy, Mater. Trans. 43 (2002) 1907-1912, <https://doi.org/10.2320/matertrans.43.1907>